

## Modeling of self-breakdown voltage statistics in high-energy spark gaps

A. L. Donaldson, M. O. Hagler, and M. KristiansenL. L. HatfieldR. M. Ness

Citation: *Journal of Applied Physics* **57**, 4981 (1985); doi: 10.1063/1.335273


View online: <http://dx.doi.org/10.1063/1.335273>

View Table of Contents: <http://aip.scitation.org/toc/jap/57/11>

Published by the *American Institute of Physics*

---

---



Small Conferences. BIG Ideas.

Applied Physics  
Reviews

SAVE THE DATE!  
**3D Bioprinting: Physical and Chemical Processes**  
May 2–3, 2017 • Winston Salem, NC, USA

The background of the banner features a blue and red 3D printed structure, possibly a biological or chemical model, with a glowing effect.

# Modeling of self-breakdown voltage statistics in high-energy spark gaps

A. L. Donaldson, M. O. Hagler, and M. Kristiansen

*Department of Electrical Engineering/Computer Science, Texas Tech University, Lubbock, Texas 79409*

L. L. Hatfield

*Department of Physics, Texas Tech University, Lubbock, Texas 79409*

R. M. Ness

*Maxwell Laboratories, 8835 Balboa Avenue, San Diego, California 92123*

(Received 28 February 1984; accepted for publication 8 January 1985)

A model which incorporates the influence of electrode surface conditions, gas pressure, and charging rate on the voltage stability of high energy spark gaps is discussed. Experimental results support several predictions of the model; namely, that increasing the pressure and the rate of voltage charging both produce a broadening of the self-breakdown voltage distribution, whereas a narrow voltage distribution can be produced by supplying a copious source of electrons at the cathode surface. Experimental results also indicate that two different mechanisms can produce this broadening, both of which can be taken into account with the use of the model presented. Further implications of the model include changes in the width of the self-breakdown voltage probability density function as the primary emission characteristics of the cathode are modified by, for example, oxide or nitride coatings and/or deposits from the insulator. Overall, the model provides a useful and physically sound framework from which the properties of spark gaps under a wide variety of experimental conditions may be evaluated.

## INTRODUCTION

Low-jitter, triggered spark gaps are needed for a wide variety of switching applications, including fusion machines,<sup>1</sup> weapons systems, and high-energy physics experiments. To achieve low jitter, the switch should be triggered as close to the self-breakdown voltage as possible. Thus, an ideal switch should have a delta function for the self-breakdown voltage probability density function. In actual operation the self-breakdown voltage will be somewhat erratic, and in most cases "prefires," or breakdown voltages which are significantly less than the mean, will occur. The self-breakdown voltage density functions and the respective distributions for these cases are shown in Fig. 1. This paper presents a model which incorporates the processes which can produce the voltage distribution shown in Fig. 1(b). The problem of prefires is not addressed here but is being considered for future work.

Numerous studies<sup>2-6</sup> have shown that the choice of gas, electrode, and insulator material can significantly influence the width and shape of the actual voltage density function. More specifically, several studies<sup>7-9</sup> have suggested a correlation of the statistical distribution in the self-breakdown voltage of a spark gap and the properties of the cathode surface, including its microstructure. The data have been interpreted in terms of models that consider:

(1) the effect of the field enhancement, due to cathode microstructure, and the effect of lower surface work functions, resulting from surface coatings, on the generation rate of electrons at the cathode<sup>7,10,11</sup>;

(2) the effect of the field enhancement on Townsend's first ionization coefficient  $\alpha$ <sup>7,12,13</sup>; and

(3) the effect of the surface coatings and the applied field on the secondary emission coefficient  $\gamma$  at the cathode.<sup>14</sup>

These models usually include the concept of "waiting-for-an-electron," in that breakdown is assumed to occur

when the first electron appears at the cathode after a breakdown condition (Townsend or Streamer condition) has been satisfied. The theoretical model presented here includes all of these mechanisms by which the cathode surface can affect

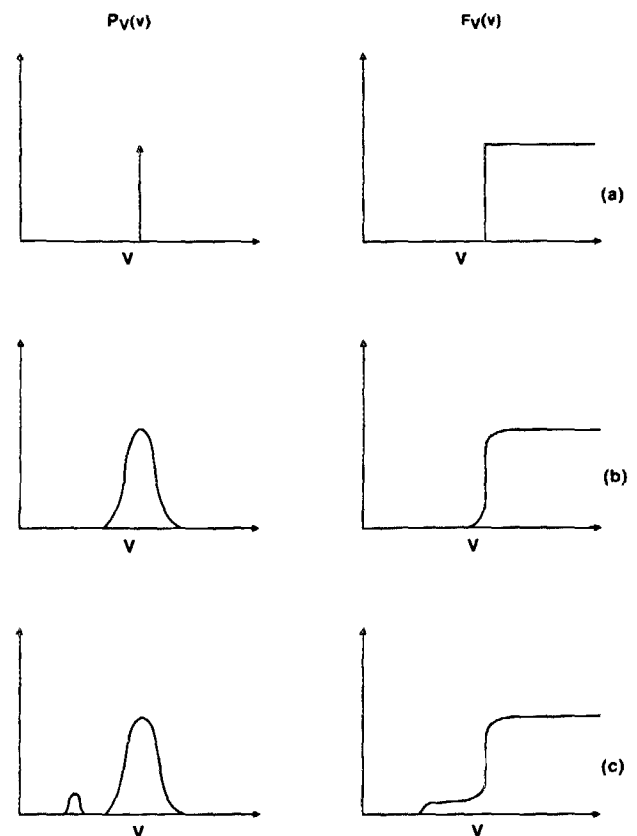


FIG. 1. Self-breakdown voltage probability density function  $p_v(v)$  and its distribution function  $F_v(v)$  for (a) ideal spark gap; (b) actual spark gap; (c) actual spark gap with prefires.

the statistical distribution in the breakdown voltage, and include the field enhancement effects on the cathode surface in a new way.

Hodges *et al.*<sup>15</sup> take into account the probability that no breakdown occurs even if the breakdown condition is satisfied. However, this probability goes from 0 to 1 quite rapidly near self-breakdown and hence is ignored for simplicity in the present analysis.

## THEORETICAL MODEL

### General case

Consider a spark gap subjected to a monotonically increasing applied voltage  $v(t)$ . Denote the breakdown voltage, a random variable, as  $V$ . The field enhancement factor  $M$ , defined as the ratio of the enhanced electric field at the cathode with microstructure to the electric field without microstructure, is also considered to be a random variable (the underlying sample space is the geometrical surface of the cathode). The random variable  $M$  is characterized by a probability density function  $p_M(m)$ . A basic assumption of the model is that the gap breaks down when an electron is born at a site on the cathode surface where  $M$  is as large as or larger than the value that satisfies the breakdown condition (perhaps Townsend or streamer) at the particular voltage applied. We denote this threshold value of the field enhancement as  $m_t(v)$ . Physically we expect that  $m_t(v)$  is a monotonically decreasing function of  $v$  [ $\partial m_t(v)/\partial v < 0$ ], an increasing function of pressure [ $\partial m_t(v)/\partial p > 0$ ], and that  $m_t(0) = \infty$  and  $m_t(v_{\max}) = 1$ . Figure 2 shows an actual calculation of  $m_t(v)$  using a model microstructure described in Appendix A. The trends for this model are listed in Table I.

We now calculate the probability  $p_t$  that the gap breaks down during the time between  $t$  and  $t + \Delta t$  and hence at a voltage between  $v$  and  $v + \Delta v$ . For  $\Delta t$  small, the probability ( $\Delta p_t$ ) that an electron is born between  $t$  and  $t + \Delta t$  at a site where  $M$  takes a value between  $m$  and  $m + \Delta m$  is

$$\Delta p_t = \frac{i_e[m, v(t)]}{e} \Delta t p_M(m) \Delta m. \quad (1)$$

The quantity  $e$  is the charge on an electron and  $i_e$  is the primary electron current generated at the cathode. In gen-

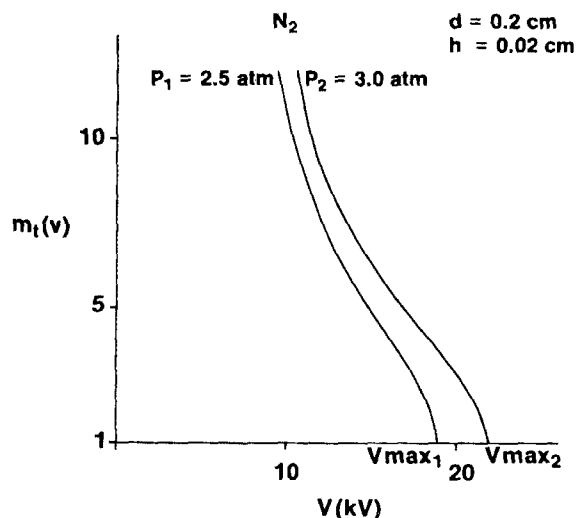


FIG. 2.  $m_t(v)$  vs  $V$  for two different pressures in nitrogen.

eral,  $i_e$  could be generated naturally by

- (a) cosmic rays ionizing the gas in front of the cathode surface,<sup>16</sup>
- (b) Fowler–Nordheim field emission,<sup>17</sup> and/or
- (c) Schottky field-assisted thermal emission.<sup>10</sup>

These emission processes could occur directly from the cathode material or from compounds existing on the cathode surface whose work function is usually lower than that of the metal and which can be effectively lowered even further by surface charging. Thus, in general,  $i_e$  could be a function of total cathode surface area, voltage, field enhancement, temperature, and work function. The last three are also functions of the position on the surface. For the following formulation, however, we will represent  $i_e$  as an explicit function of field enhancement and voltage only (see Appendix B).

If  $\Delta t$  is large compared with the time of avalanche formation (see Appendix C), then the probability that the gap breaks down between  $t$  and  $t + \Delta t$  is

$$p_t(\Delta t) = \frac{\Delta t}{e} \int_{m_t(v)}^{\infty} i_e[m, v(t)] p_M(m) dm. \quad (2)$$

TABLE I. General trends for the threshold field enhancement  $m_t(v)$  calculated for an ellipsoidal protrusion in a uniform field using the Townsend breakdown criteria in  $N_2$  and the streamer criteria in  $SF_6$ .

| Trend   | Implication   |
|---|---|
| T-1: $\frac{\partial v}{\partial m_t} > 0$  | The greater the spread in field enhancements, the greater the possible range in breakdown voltages.                             |
| T-2: $\frac{\partial m_t}{\partial p} > 0$  | The higher the pressure, the higher the required threshold field enhancement for a fixed voltage.                               |
| T-3: $\frac{\partial}{\partial p} \left( \frac{\partial v}{\partial m_t} \right) > 0$ | For a fixed distribution of field enhancements, the higher the pressure, the greater the possible spread in breakdown voltages. |
| T-4: $\frac{\partial}{\partial d} \left( \frac{\partial v}{\partial m_t} \right) < 0$ | The larger the gap spacing, the smaller the effect of surface microstructure.   |
| T-5: $\frac{\partial}{\partial h} \left( \frac{\partial v}{\partial m_t} \right) > 0$ | The larger the microstructure, the greater the spread in breakdown voltage for a fixed distribution of field enhancements.      |

Note: All trends for  $SF_6$  are greater than and in the same direction as the trends for nitrogen.

Let the random variable  $T$  represent the time elapsed before breakdown of the gap. Then, from Eq. (2), the probability density function for  $T$  is readily seen to be<sup>18</sup>

$$p_T(t) = f(t) \exp\left(-\int_0^t f(\tau) d\tau\right), \quad (3)$$

where

$$f(t) = \frac{1}{e} \int_{m_i(v(t))}^{\infty} i_e[m, v(t)] p_M(m) dm. \quad (4)$$

Since, by assumption,  $v(t)$  is a monotonic function of  $t$ , then the probability density function for the breakdown voltage  $v$  is<sup>19</sup>

$$p_V(v) = p_T[t(v)] \left| \frac{dv}{dt} \right| \quad (5)$$

$$p_V(v) = \frac{\lambda(v)}{v'} \exp\left(-\int_0^v \frac{\lambda(\eta) d\eta}{v'}\right), \quad (6)$$

where  $v'$  is the derivative of the charging voltage with respect to time  $[dv(t)/dt]$  and

$$\lambda(v) = \frac{1}{e} \int_{m_i(v)}^{\infty} i_e(m, v) p_M(m) dm. \quad (7)$$

It is easy to see that

$$F_V(v) = \int_0^v p_V(\xi) d\xi = 1 - \exp\left(-\int_0^v \frac{\lambda(\eta) d\eta}{v'(\eta)}\right), \quad (8)$$

where  $F_V(v)$  is the cumulative probability distribution for the random variable,  $V$ . Equation (8) shows that the width of the self-breakdown voltage distribution (1) decreases with increasing  $i_e$ , (2) increases with increasing  $m_i$ , caused by, for example, an increase in operating pressure, and (3) increases with increasing  $v'$ , the charging rate. Note that  $v'$  is to be evaluated at  $v$ , and hence can be considered as a function of  $v$ , namely,  $v' = v'(v)$ . If  $v(t)$  is a ramp, then  $v' = v'_0$ , a constant. If  $v(t)$  is an  $RC$  charging waveform, then  $v' = (v_0 - v)/RC$ , where  $v_0$  is the charging voltage. If  $v(t) = A(1 - \cos \omega t)$  for  $0 < \omega t < \pi$ , then  $v' = \omega \sqrt{v(2A - v)}$ .

From Eqs. (7) and (8), it is easy to show<sup>20</sup> that

$$\lambda(v) = \frac{1}{e} \int_{m_i(v)}^{\infty} i_e(m, v) p_M(m) dm = \frac{v' p_V(v)}{1 - F_V(v)}. \quad (9)$$

Notice that all the terms on the right-hand side of Eq. (9) can be measured experimentally. This will hold true for the special cases discussed below as well. This is an important result, for even when  $i_e$  depends on (implicit) variables other than  $m$  and  $v$ , the function  $v' p_V(v) / [1 - F_V(v)]$  should still describe the results (see Appendix B).

### Special cases

To proceed further, consider two special cases of the model. First, suppose that  $i_e(m, v)$  is constant so that field-enhancement distribution effects from the cathode surface microstructure and waiting-for-an-electron effects are the primary physical mechanisms included in the model. This circumstance is likely to hold, for example, when the cathode is illuminated with sufficiently intense ultraviolet radiation so that any field emission current is dwarfed by photoelectric current, which should be independent of  $M$  and  $V$ . If  $i_e = i_{e0}$ , a constant, then Eq. (9) gives

$$\lambda(v) = \frac{i_{e0}}{e} \{1 - F_M[m_i(v)]\} = \frac{v' p_V(v)}{1 - F_V(v)}, \quad (10)$$

where  $F_M(m)$  is the cumulative probability distribution for the random variable  $M$ . If we know  $m_i(v)$ , we can determine  $F_M(m)$  by plotting  $F_M[m_i(v)]$  vs  $m_i(v)$ . Therefore, for this special case it is possible, in principle, to deduce  $F_M(m)$  from  $p_V(v)$  (self-breakdown voltage histogram) under a given set of conditions and thus predict  $p_V(v)$  [or  $F_V(v)$ ] for a different  $v'$  or gas pressure [which affects  $m_i(v)$ ], for example. For this special case, Eq. (8) becomes

$$F_V(v) = 1 - \exp\left(-\frac{i_{e0}}{e} \int_0^v \frac{\{1 - F_M[m_i(\eta)]\} d\eta}{v'}\right). \quad (11)$$

Consider now a second special case in which  $p_M(m) = \delta(m - m_0)$ , where  $\delta(\cdot)$  is the Dirac delta function and  $m_0$  is a constant. In this case the field enhancement is assumed to be uniform (that is, sufficiently characterized by its mean value rather than its distribution) so that the primary effects included are the voltage dependence of the primary electron current  $i_e$  and waiting-for-an-electron. In this case Eq. (8) becomes

$$F_V(v) = 1 - \exp\left(-\frac{1}{e} \int_{v_i}^v \frac{i_e(m_0, \eta) d\eta}{v'}\right), \quad (12)$$

where  $v_i$  is the threshold voltage, and  $m_i(v_i) = m_0$ , while Eq. (9) becomes

$$\lambda(v) = \frac{i_e(m_0, v)}{e} = \frac{v' p_V(v)}{1 - F_V(v)}, \quad v > v_i. \quad (13)$$

### EXPERIMENTAL ARRANGEMENT

The experimental arrangement and the system diagnostics used to test the theoretical results are shown in Figs. 3 and 4. The construction of this facility and the development of the modeling software is described elsewhere.<sup>9,21</sup> The test circuit shown in Fig. 4 consists of a high-energy (2 kJ) pulse-forming network (PFN) and a low-energy (< 1 mJ)  $RC$  probing circuit. The PFN delivers a unipolar, 25- $\mu$ sec pulse into a 0.6- $\Omega$  matched load in order to generate an electrode surface which is characteristic of a high-energy switch. The  $RC$  probing circuit is used to generate the voltage distributions with a low-energy, low-current pulse so that the equilibrium

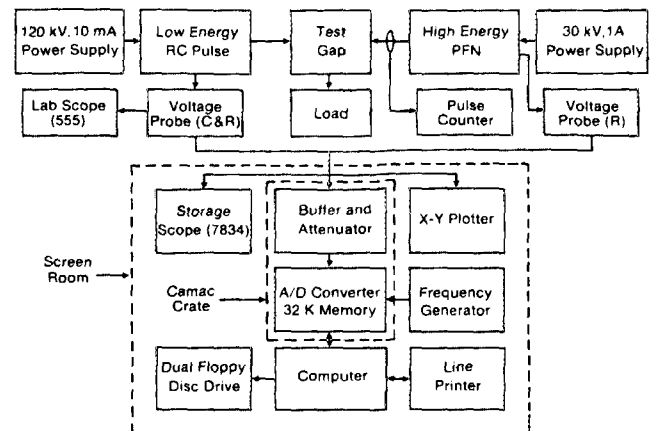


FIG. 3. Experimental arrangement and system diagnostics.

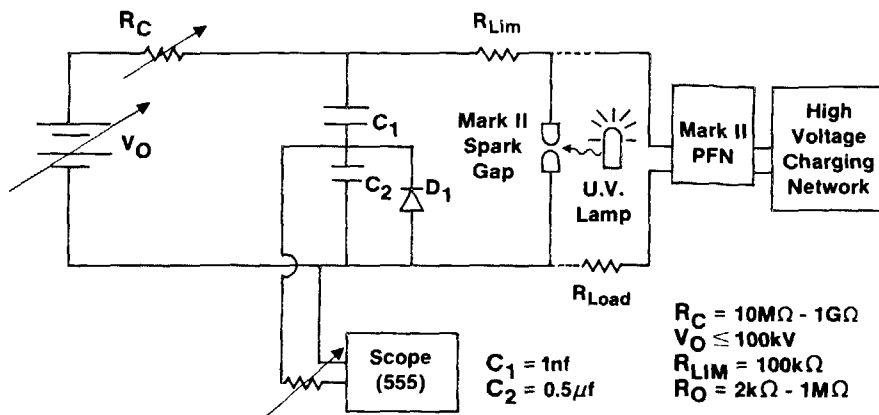


FIG. 4. Test circuits.

temperature is reached prior to each shot. This low-energy circuit is also used so that the surface microstructure produced by the high-energy shots will not be altered significantly from shot to shot. The criteria for determining that no alteration in surface features had occurred was the comparison of the voltage distributions before and after a given experiment. The pressure in the spark gap could be raised to 3.5 atm and the voltage ramp rate could be varied from 3 to 60 kV/s by changing  $R_c$ . A 5-W UV lamp was used to gener-

ate additional electrons at the cathode surface when needed.

A testing sequence consisted of firing 2000–7000 shots at high energy, waiting approximately 1 h for the electrode to cool, and proceeding with several series of 500 low energy shots with different  $i_e$ ,  $v'$ , and pressure. The Kolmogorov–Smirnov<sup>22</sup> test indicates that this number of shots should determine  $F_V(v)$ , within a confidence level of 99%, to an accuracy of 7%. Figure 5 shows a typical electrode surface generated by the high-energy pulses for the case of 304 stainless-steel run in one atmosphere of nitrogen gas at a gap separation of 5 mm. Examination of the electrode surface after application of the low-energy pulses indicates that no significant changes had occurred which might alter the breakdown statistics.

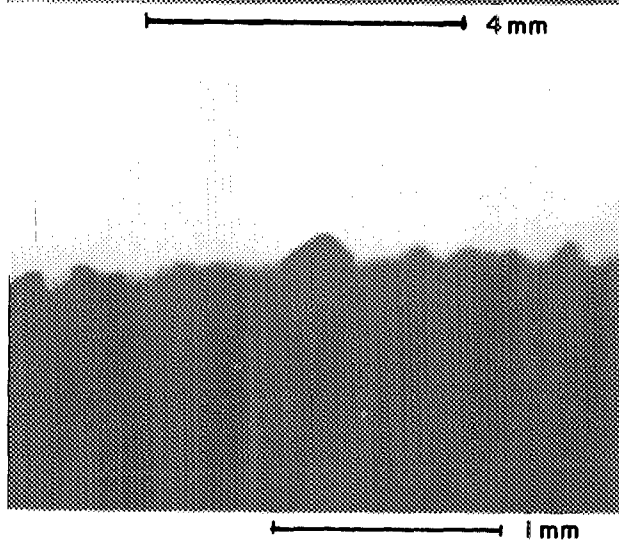
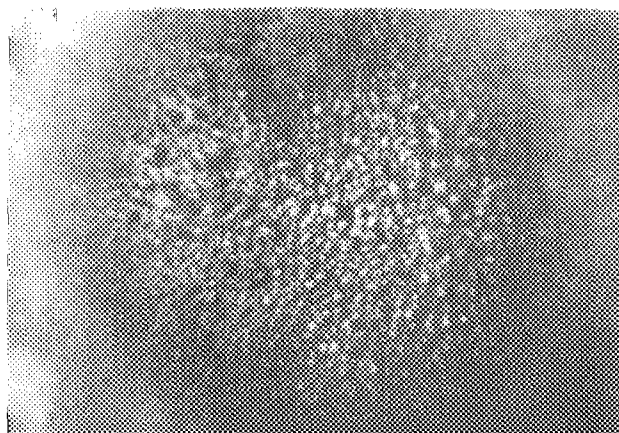


FIG. 5. Stainless-steel electrode after 2200 high-energy discharges in nitrogen: (a) cathode surface—top view (marker is 4 mm); (b) cathode surface—side view (marker is 1 mm).

## EXPERIMENTAL RESULTS

Several experiments were performed to verify the model's predictions for the effect of  $i_e$ ,  $v'$ , and pressure on the probability density function  $p_V(v)$ . In the first experiment, an UV source was used to generate a continuous supply of photoelectrons at the surface of a stainless steel electrode in air. Figure 6 shows that, without UV, the density function is very broad, indicating that the cathode surface is a very poor emitter of electrons. However, with the UV source on, the density function is reduced and shifts to the lowest value of breakdown voltage. Nitta *et al.*<sup>23</sup> observed the same effect in SF<sub>6</sub> at pressures up to 2 atm. This result is significant for at least two reasons. First, it supports the waiting-for-an-electron concept as one mechanism responsible for statistical

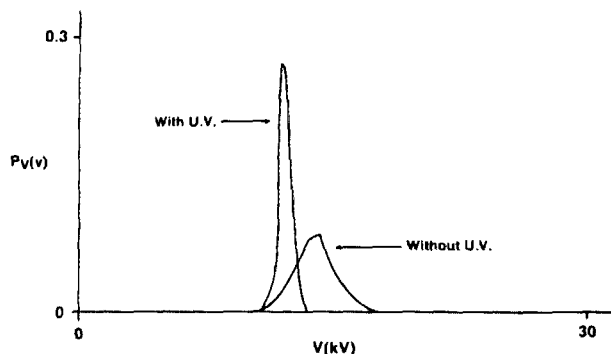


FIG. 6. Self-breakdown voltage probability density function for stainless steel in air, with and without UV.

variation in the self-breakdown voltage; and second, it provides an externally controllable experimental "switch" where the effect of waiting-for-an-electron can be turned on or off. The behavior observed is consistent with Eq. (8).

A second experiment consisted of varying the voltage ramp rate  $v'$  from 3 kV/s ("slow" ramp) to 30 kV/s ("fast" ramp). According to the model [Eq. (8)], if you are waiting for an electron to appear, then the faster the ramp rate, the higher the breakdown voltage will be when the electron appears and thus the greater the scatter in the density function  $p_V(v)$ . Figure 7 shows that this effect was indeed observed. Also, from Eq. (8), the density function for the slower ramp rate could be theoretically calculated from the data for the fast ramp rate. Figure 7 shows this result for the assumption  $i_e = i_{e0}$ , a constant. The result is fair, indicating that for better agreement a more realistic expression for  $i_e$ , perhaps  $i_e(m, v)$ , would have to be used. Hodges<sup>10,11</sup> has modeled this effect using  $i_e(m, v, \phi, \theta)$  and was able to achieve good agreement between experimental and theoretical values.

Previous work<sup>13,24-26</sup> has shown that with the presence of cathode microstructure, an increase in pressure can lead to significant deviations from the Paschen curve breakdown voltage if the product of the protrusion height and the pressure is greater than a gas-dependent threshold. For example, Berger<sup>13</sup> calculated that pressure-height products of 30  $\mu\text{m atm}$  for  $\text{SF}_6$  and 200  $\mu\text{m atm}$  for air would be required for the onset of breakdown voltage modifications due to enhanced ionization occurring near the microprotrusions. Avrutskii<sup>8</sup> stated that an increase in pressure should lead to an increase in scatter in the breakdown voltage, but no data were given. Thus, in order to understand the effect of pressure on the breakdown voltage statistics for a surface with large protrusions, the brass sample shown in Fig. 8 was generated and the breakdown voltages were recorded for pressures up to 3.5 atm. (Earlier work in electrode erosion showed that brass electrodes in high energy operation can form protrusions up to 500  $\mu\text{m}$ .<sup>21</sup>) Figure 9 clearly shows an increase in scatter, especially at the low end, in the density function  $p_V(v)$  for higher pressures. If the effect is due to field enhancements, then the calculated range of  $m$ 's at any pressure should be the same since the distribution of surface field enhancements is not changing from shot to shot. For  $p = 1.7$  atm, the range of  $m$ 's, calculated using the model in Appendix A, was 1-2.93; for  $p = 2.5$  atm, the range was 1-3.63.

Increased scatter with increased pressure has also been

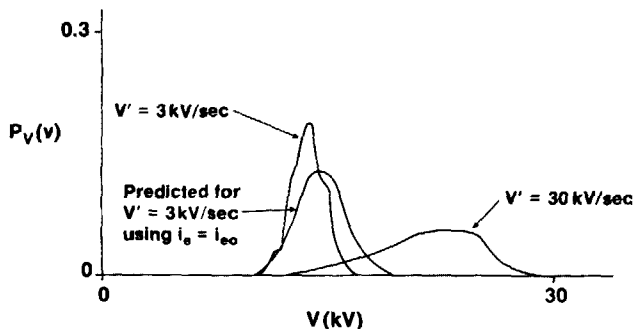


FIG. 7. Self-breakdown voltage probability density function for different charging rates.

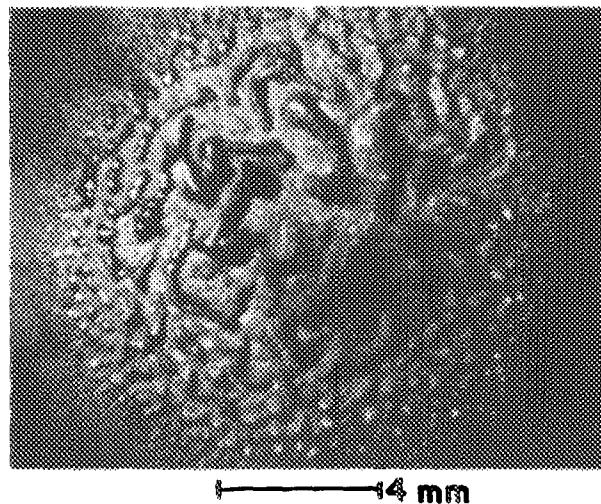


FIG. 8. Surface of brass cathode used for pressure studies (marker is 4 mm).

observed for electrode surfaces with microstructures much smaller than the size required to affect the breakdown voltage. Figure 10 shows the breakdown voltage distribution as a function of pressure for graphite electrodes in air. The entire electrode surface was examined with a high-power optical microscope and no protrusions greater than 10  $\mu\text{m}$  were discovered. Although the pressure-height product is an order of magnitude less than the amount required to affect the breakdown voltage by enhanced ionization,<sup>13</sup> there is still a significant spreading of the distribution at higher pressures. Unlike the results for the brass electrodes, the spreading occurs at the high end of the distributions, i.e., for voltages larger than those calculated from the Townsend breakdown criteria for a gap without protrusions, and  $M = 1$ . Whereas the results for brass indicated a lowering of the Townsend breakdown criteria due to enhanced ionization, the results for graphite suggest that a different mechanism is producing the scatter at high pressures, possibly, by altering the effective generation rate of electrons. Levinson and Kunhardt<sup>27</sup> have reported a reduction in the effective electron generation rate at the cathode for higher pressures, although no specific mechanism was described.

The pressure data were also found to be of importance for analyzing the different  $i_e$  cases which were studied theor-

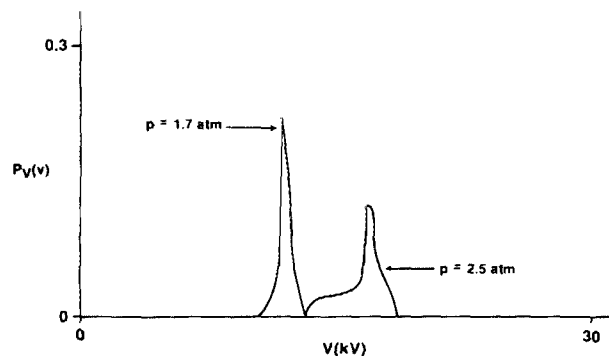


FIG. 9. Self-breakdown voltage probability density function for brass electrodes in air at different pressures.

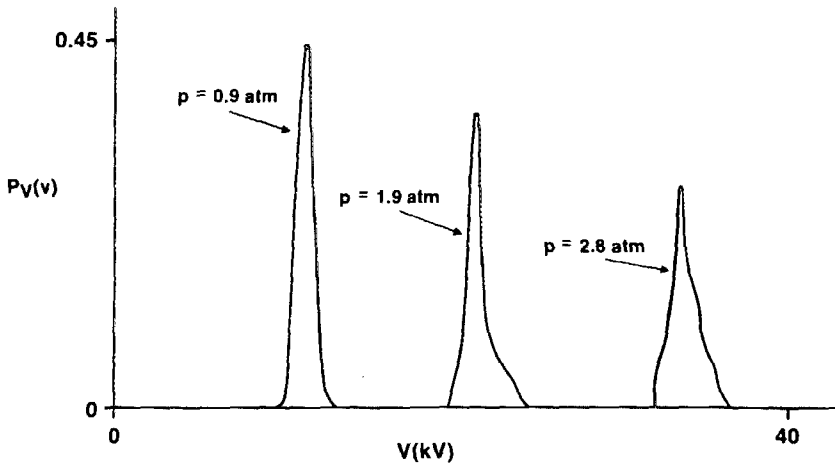


FIG. 10. Self-breakdown voltage probability density function for graphite electrodes in air at different pressures.

etically. Figure 11 shows theoretical plots of the quantity  $v'p_V(v)/[1 - F_V(v)]$  for the three physical cases discussed earlier: (a)  $i_e = i_e(m_0, v)$ ,  $m_0$  is a constant over the entire surface [Eq. (13)]; (b)  $i_e = i_{e0}$  is a constant [Eq. (10)]; and (c) the most general case,  $i_e = i_e(m, v)$  which assumes a distribution of surface field enhancements [Eq. (9)]. A Gaussian distribution in field enhancements was used for cases (b) and (c). The function  $m_t(v)$  was calculated using the model described in Appendix A and a Schottky emission current was used for  $i_e(m, v)$ . Case (a) illustrates that if there is no spread in the distribution for  $M$  [Eq. (13)], then an increase in pressure will correspond simply to a higher emission current because of the higher breakdown voltage occurring at that pressure, which is typical for a field-dependent Schottky or Fowler-Nordheim emission mechanism.<sup>10</sup> A higher emission current at higher pressure would imply narrower statistics, but experimental results indicate just the opposite; namely, broader statistics at higher pressures. However, in case (b) for a fixed voltage, the increase in pressure has the effect of raising the threshold  $m_t$  required for breakdown which raises  $F_M[m_t(v)]$ , and thus the function  $v'p_V(v)/[1 - F_V(v)]$  is multivalued and decreases with increasing pressure [Eq.

(10)]. For case (c),  $v'p_V(v)/[1 - F_V(v)]$  is also multivalued and decreases with increasing pressure, but in a different way [Eq. (9)]. For a fixed voltage, and assuming that the surface features do not change with pressure, the integrand is constant with increasing pressure. However, the lower limit on the integral, namely  $m_t(v)$ , increases with increasing pressure which has the effect of reducing the value of the function.

Figure 12 is a plot of the function  $v'p_V(v)/[1 - F_V(v)]$  from experimental data for the pressure data of Fig. 9. From this plot it is clearly seen that the experimental data are inconsistent with the theoretical results for case (a) (a constant  $M$  surface). Thus, the effect of a distribution in field enhancements should be considered in the analysis of the breakdown statistics. In addition, the function  $v'p_V(v)/[1 - F_V(v)]$  increases very rapidly with voltage and only very extreme values for the work function,  $\Phi < 0.5$  eV, and field enhancement,  $M > 50$ , could give reasonable agreement between the experimental data and the Fowler-Nordheim or Schottky field emission mechanisms.

## CONCLUSION

A model has been described which correctly accounts for the influence of pressure,  $v'$ ,  $i_e$ , and surface microstructure on the self-breakdown voltage statistics. The model's importance in the area of pulse-charged and triggered switches stems from the fact that the statistics for these systems have been recently shown<sup>28</sup> to be heavily dependent on the self-breakdown statistics discussed in this paper.

Using this model, theoretical and experimental results show:

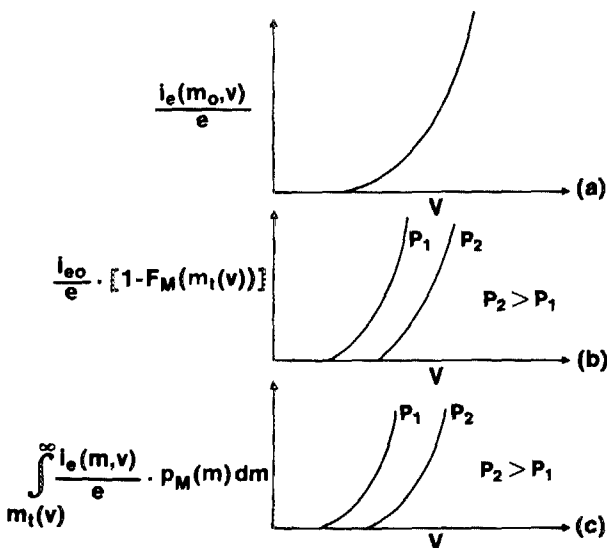


FIG. 11. Theoretical plots of  $v'p_V(v)/[1 - F_V(v)]$  for (a)  $i_e = i_e(m_0, v)$ ; (b)  $i_e = i_{e0}$ ; and (c)  $i_e = i_e(m, v)$ .

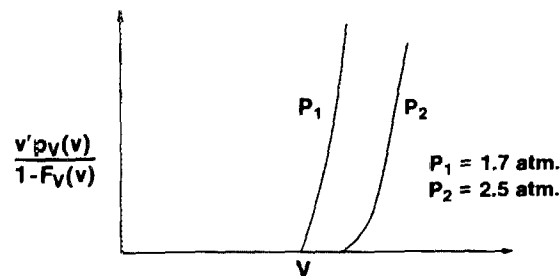


FIG. 12. Experimental plots of  $v'p_V(v)/[1 - F_V(v)]$ .

(1) The spread in self-breakdown voltages in a spark gap is a function of the charging rate ( $v'$ ) and the cathode surface properties which determine the electron emission current  $i_e$  and the distribution of field-enhancement sites  $F_M(m)$ .

(2) Increasing  $i_e$  provides a practical method for reducing the width of the self-breakdown voltage density function. This can be accomplished with an external UV source, by sandblasting the electrodes to supply a large number of low work-function emitting sites,<sup>28</sup> or perhaps with an electron emission agent introduced into the cathode material.<sup>29</sup>

(3) The spread in self-breakdown voltages increases with increasing pressure, and/or increasing charging rate.

(4) Increasing pressure had two distinctive effects on the breakdown voltage distributions. For large microstructures ( $> 200 \mu\text{m}$ ) on brass electrodes, increasing pressure led to increased scatter at the lower end of the distributions as a result of enhanced ionization near the microprotrusions. For small microstructures ( $< 10 \mu\text{m}$ ) on graphite electrodes, an increase in pressure led to increased scatter at the high end of the distributions which perhaps was due to a lowering of the effective electron emission current  $i_e$ .

(5) The function  $v'p_v(v)/[1 - F_v(v)]$ , which can be compared directly from self-breakdown voltage data, is useful for determining the nature of  $i_e$  for a given set of conditions.

#### ACKNOWLEDGMENTS

The authors are indebted to B. Conover, P. Krothapalli, K. Rathbun, and A. Shaukat for their work on the construction of the experiment and the implementation of the data acquisition system. In addition, a special thanks goes to M. Byrd, J. Clare, R. Davis, L. Heck, R. Higgenbotham, M. Katsaras, and M. C. McNeil for their work on the manuscript. This work was supported by the Air Force Office of Scientific Research.

#### APPENDIX A

The Townsend breakdown criterion for a spark gap with microstructure is given by

$$\int_h^d \bar{\alpha} dz = K, \quad (\text{A1})$$

where  $\bar{\alpha}$  is the effective ionization coefficient of the gas which is equal to  $\alpha - \eta$ ; where  $\alpha$  is the Townsend first ioni-

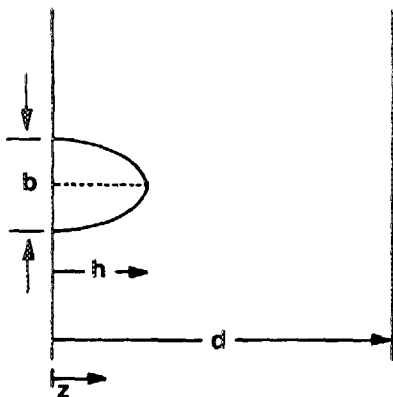


FIG. A1. Ellipsoidal surface protrusion model.

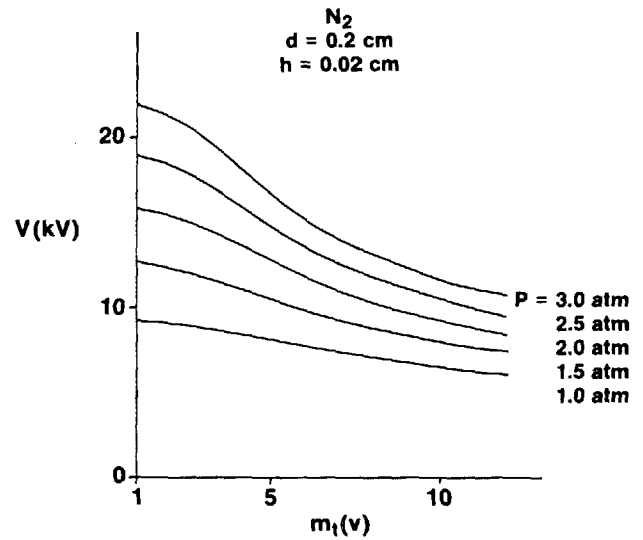


FIG. A2.  $m_1(v)$  vs  $V$  as a function of pressure in nitrogen.

zation coefficient,  $\eta$  is the attachment coefficient,  $h$  is the protrusion height,  $d$  is the gap spacing, and  $K$  is a function of  $E/p$  which is obtained from empirical data. The microstructure modifies the voltage which satisfied Eq. (A1) by altering the electric field and thus  $\bar{\alpha}$  in the region near the protrusion. One can model the protrusion several ways,<sup>12,30</sup> but the semiellipsoidal model shown in Fig. A1 was chosen because the electric field along the  $z$  axis was known analytically and could be expressed in terms of the field-enhancement  $M$ . The axial field for this configuration is given by<sup>12</sup>

$$E(z) = E_0 \left( 1 + (M - 1) \frac{h^3}{z^3} \right), \quad (\text{A2})$$

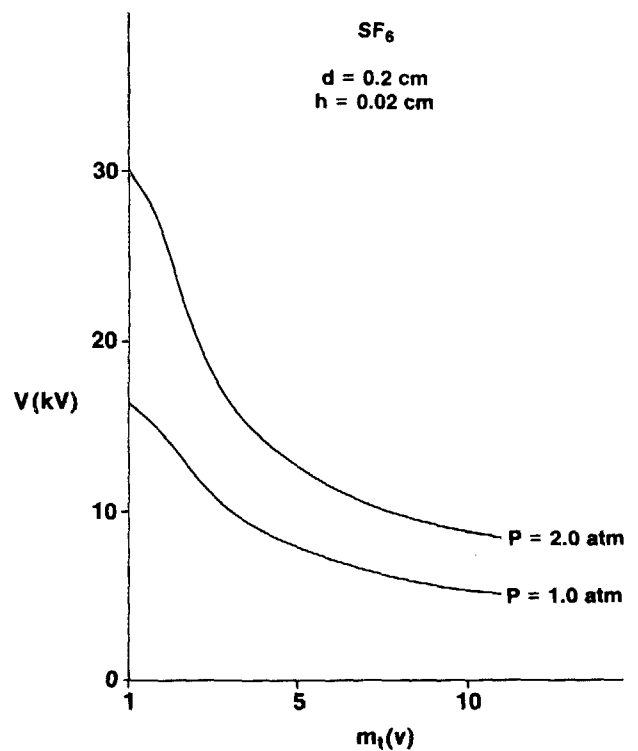


FIG. A3.  $m_1(v)$  vs  $V$  as a function of pressure in  $\text{SF}_6$ .



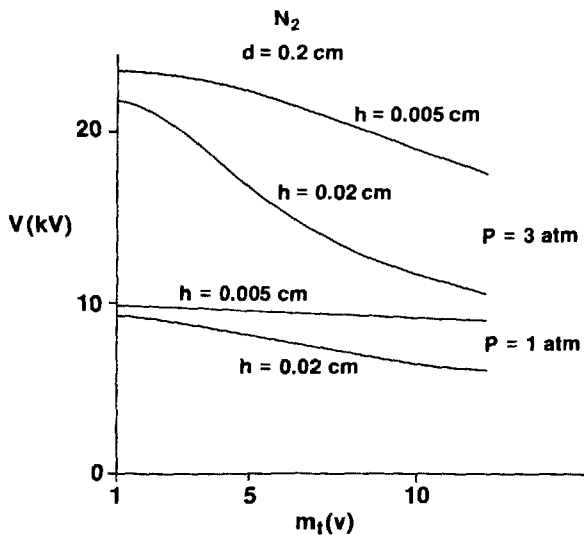


FIG. A4.  $m_1(v)$  vs  $V$  as a function of protrusion height for two different pressures in nitrogen.

where  $E_0$  is the electric field with no protrusions.

The field-enhancement factor  $M$  is related to  $b$ , the radius of the base of the protrusion, and  $h$ , the protrusion height, by the equation

$$M = \frac{c^2}{1-c^2} \left( \frac{1}{2c} \ln \frac{1+c}{1-c} - 1 \right)^{-1}, \quad (\text{A3})$$

where

$$c = 1 - b^2/h^2.$$

The coefficients  $\bar{\alpha}$  and  $K$  were obtained from the literature.<sup>13,31</sup> Thus, Eq. (A1) was solved for a variety of conditions and plotted in Figs. A2–A4. It should be remembered that these graphs are useful only for showing trends since actual surface structure effects are not as simple as a single ellipsoid. Also, it was assumed that  $\bar{\alpha}$  takes on its equilibrium value instantly, when in reality it would gradually approach its equilibrium value within a few collision paths.<sup>32</sup> This effect is depicted in Fig. A5 and the calculated results in Fig. A6 show that if one takes this into account the effect would be to smooth the surface out or to reduce protrusion effects. The actual transition was calculated using an  $\alpha$  which reached equilibrium in a linear manner. Any monotonic

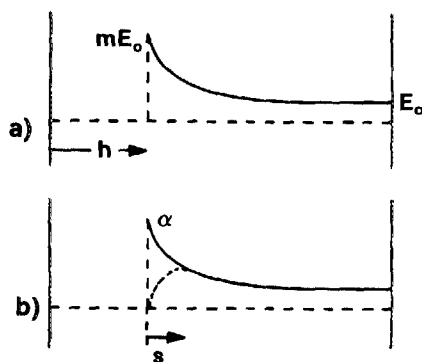


FIG. A5. (a) Electric field across the gap; (b)  $\alpha$  with and without correction factor for nonequilibrium values over a distance  $S$ .

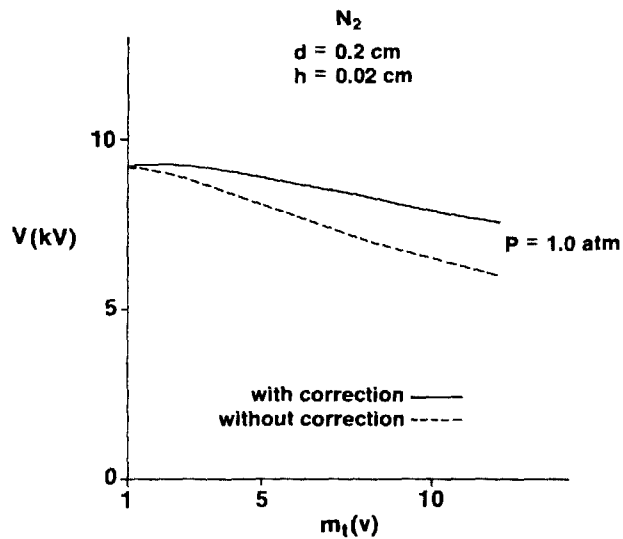


FIG. A6.  $m_1(v)$  vs  $V$  with and without equilibrium  $\alpha$  correction in nitrogen.

transition function, however, would have a similar effect.

Thus, the values obtained for the breakdown voltage using equilibrium values of  $\bar{\alpha}$  are lower limits for a given set of conditions.

## APPENDIX B

Suppose that the primary electron current  $\bar{i}_e$  depends on the random variables,  $\Theta$ , the temperature over the cathode surface, and  $\Phi$ , the work function over the cathode surface, in addition to the random variable  $M$  and the applied voltage  $v(t)$ . Then Eq. (2) becomes

$$p_r(\Delta t) = \frac{\Delta t}{e} \int_0^\infty d\phi \int_0^\infty d\theta \int_{m_1(v)}^\infty \bar{i}_e[\phi, \theta, m, v(t)] \times p_{\Phi\Theta M}(\phi, \theta, m) dm,$$

where  $p_{\Phi\Theta M}(\phi, \theta, m)$  is the joint probability density function for  $\Phi$ ,  $\Theta$ , and  $M$ . Since<sup>33</sup>

$$p_{\Phi\Theta M}(\phi, \theta, m) = p_M(m) p_\Phi(\phi | m) p_\Theta(\theta | m, \phi),$$

where  $p_\Phi(\phi | m)$  and  $p_\Theta(\theta | m, \phi)$  are conditional probability densities, then

$$p_r(\Delta t) = \frac{\Delta t}{e} \int_{m_1(v)}^\infty i_e[m, v(t)] p_M(m) dm,$$

where

$$i_e[m, v(t)] \equiv \int_0^\infty d\phi \int_0^\infty d\theta \bar{i}_e[\phi, \theta, m, v(t)] \times p_\Phi(\phi | m) p_\Theta(\theta | m, \phi).$$

Clearly, the form of  $p_r(\Delta t)$  does not change when the dependence of the current on the additional random variables,  $\Phi$  and  $\Theta$ , is included. The dependence of the current on the random variable  $M$  is important, on the other hand, because the limits of the integral over  $m$  are not fixed, but depend on  $m_1(v)$ , a quantity that depends on the breakdown criterion, Townsend or streamer. The work function over the surface  $\Phi$  and the temperature over the surface  $\Theta$  do not enter into the breakdown criterion, however, and hence are important only in an average sense in this formulation.

Note that the various probability densities are assumed constant in time. This assumption seems implausible for the temperature  $\theta$  until we realize that it is the temperature probability density at the time of breakdown that matters, and that the time between breakdowns is nearly constant so that the temperature probability density should be essentially the same for each shot.

It is instructive to consider  $M$ ,  $\phi$ , and  $\theta$ , as random processes,<sup>34</sup> not in time, but in the spatial variables that describe the cathode surface. The sample functions of these processes are the spatial distributions of field enhancement, surface work function, and surface temperature after each shot, just before the next breakdown. Particularly for other than planar electrodes, we expect each process to be spatially nonstationary.<sup>35</sup> In that case, the probability densities, the primary current density  $j_e$  and the field-enhancement threshold  $m_t$ , become functions of the spatial variables  $\sigma$  that describe the cathode surface. Let the primary electron current density be  $j_e[\phi, \theta, m, v(t); \sigma]$  where we set off the spatial dependence with a semicolon; then Eq. (2) becomes

$$p_i(\Delta t) = \frac{\Delta t}{e} \int_{\Sigma} d\sigma \int_{m_t, v, \sigma}^{\infty} dm \int_0^{\infty} d\phi \bar{j}_e[\phi, \theta, m, v(t); \sigma] \times p_{\phi\theta M}(\phi, \theta, m; \sigma),$$

where  $\Sigma$  is the cathode surface. Or

$$p_i(\Delta t) = \frac{\Delta t}{e} \int_{\Sigma} d\sigma \int_{m_t, v, \sigma}^{\infty} j_e[m, v(t); \sigma] p_M(m; \sigma) dm,$$

where

$$j_e[m, v(t); \sigma] \equiv \int_0^{\infty} d\phi \int_0^{\infty} d\theta \bar{j}_e[\phi, \theta, m, v(t); \sigma] \times p_{\phi}(\phi | m; \sigma) p_{\theta}(\theta | m, \phi; \sigma).$$

The corresponding value of  $\lambda(v)$  is

$$\lambda(v) = \frac{1}{e} \int_{\Sigma} d\sigma \int_{m_t, v, \sigma}^{\infty} j_e(m, v; \sigma) p_M(m; \sigma) dm.$$

Consider, as an example, a spark gap with hemispherical electrodes and let  $\sigma = \sigma_0$  correspond to the point on the surface at the center of the gap where the distance between the electrodes is a minimum. As we move further away from the center of the cathode,  $j_e$  tends to remain constant (if it results from photoemission) or decrease (if it results from Schottky or Fowler-Nordheim emission) because the electric field at the cathode surface decreases as we move away from the electrode center. For a given relatively high value of  $m$ ,  $p_M(m; \sigma)$  should decrease sufficiently far away from electrode center as the cathode surface becomes smoother. The threshold field enhancement  $m_t(v; \sigma)$ , on the other hand, will increase rapidly as we move away from cathode center because  $m_t$  increases rapidly with the increasing distance between electrodes. Thus, the integral over  $m$  decreases rapidly as we move away from  $\sigma_0$ . That is, the contributions to  $\lambda(v)$  come primarily from a small area  $\delta A$  near the electrode center  $\sigma_0$ . Thus,

$$\lambda(v) = \int_{m_t, v, \sigma_0}^{\infty} i_e(m, v; \sigma_0) p_M(m; \sigma_0) dm,$$

where

$$i_e(m, v; \sigma_0) = j_e(m, v; \sigma_0) \delta A.$$

This result is the same as Eq. (7) if we, in Eq. (7), use  $i_e$ ,  $p_M$ , and  $m_t$ , corresponding to conditions near the cathode center. The use of these quantities appropriate to the central region is consistent with empirical observations that almost all breakdowns occur in this region.

## APPENDIX C

In the main body of the paper, it was assumed that the time for avalanche formation (formative time) is sufficiently short so that the applied voltage changes only negligibly ( $< 100$  V) during this time. For SF<sub>6</sub> and air at 1 atm, the maximum formative times are approximately  $100 \mu\text{s}$ <sup>36,37</sup> and thus, for charging rates less than  $1000$  kV/s, this assumption is valid.

If the formative time is not negligible, then it is considered to be a random variable  $T \dagger$  with a probability density  $p_{T \dagger}(t)$ . The increase in applied voltage during  $T \dagger$  is a random variable  $V \dagger$ . Because the voltage and time are monotonically related<sup>18</sup>

$$p_{V \dagger}(v) = p_{T \dagger}(t) / |dv/dt|. \quad (C1)$$

Under these circumstances, the gap breakdown voltage is not simply  $V$ , the applied voltage when the first electron is born at a site at the cathode surface where  $M > m_t$ , but rather the sum of  $V$  and  $V \dagger$ , which will be called  $U$ .

$$U = V + V \dagger. \quad (C2)$$

Thus,  $U$  is the sum of two random variables. Its probability density is therefore given by<sup>38</sup>

$$p_U(v) = \int_{-\infty}^{\infty} p_{V, V \dagger}(v - u, u) du, \quad (C3)$$

where  $p_{V, V \dagger}(v, u)$  is the joint probability density for  $V$  and  $V \dagger$ . If  $V$  and  $V \dagger$  are statistically independent, then this result simplifies to<sup>39</sup>

$$p_U(v) = p_V(v) * p_{V \dagger}(v), \quad (C4)$$

where the asterisk denotes convolution in  $v$ ,  $p_V(v)$  is given by Eq. (6), and  $p_{V \dagger}(v)$  is found using Eq. (C1). The random variables  $V$  and  $V \dagger$  are simply transformations of  $T$  and  $T \dagger$ . Therefore,<sup>40</sup>  $V$  and  $V \dagger$  will be statistically independent if the formative time  $T \dagger$  does not depend on the time  $T$  required for an electron to be born at a site on the cathode surface where  $M > m_t$ .

Notice that if the formative time is negligible, then  $p_{V \dagger}(v)$  becomes  $\delta(v)$ , a Dirac delta function, so that

$$p_U(v) = p_V(v) * \delta(v) = p_V(v). \quad (C5)$$

This case is the one assumed in the body of the paper.

<sup>1</sup>R. A. White, Proceedings of the 3rd IEEE International Pulsed Power Conference, Albuquerque, NM June, 1981, p. 359.

<sup>2</sup>L. B. Gordon, M. Kristiansen, M. O. Hagler, H. C. Kirbie, R. M. Ness, L. Hatfield, and J. N. Marx, IEEE Trans. Plasma Sci. PS-10, 286 (1982).

<sup>3</sup>E. I. Zolotarev, V. Mukhin, L. E. Polyanskii, and V. N. Trapeznikov, Sov. Phys. Tech. Phys. 21, 340 (1978).

<sup>4</sup>Physics International Report PISR-127-4, Physics International Co., 2700 Merced Street, San Leandro, CA 94577 (July 1969).

<sup>5</sup>M. T. Buttram, Sandia National Lab Report, Sand 81-1552 (1981).

- <sup>6</sup>T. H. Martin, Air Force Pulsed Power Lecture Note No. 11, Plasma and Switching Laboratory, Department of Electrical Engineering, Texas Tech University (1983).
- <sup>7</sup>V. A. Avrutskii, *Sov. Phys. Tech. Phys.* **18**, 389 (1973).
- <sup>8</sup>V. A. Avrutskii, G. M. Goncharenko, and E. N. Prokharov, *Sov. Phys. Tech. Phys.* **18**, 386 (1973).
- <sup>9</sup>R. M. Ness, Masters Thesis, Texas Tech University (August 1983).
- <sup>10</sup>R. V. Hodges, R. C. McCalley, and J. F. Riley, Lockheed Missiles and Space Company Report, LMSC-D811978 (1982).
- <sup>11</sup>R. V. Hodges and J. F. Riley, Lockheed Missiles and Space Company Report, LMSC-D877208 (1983).
- <sup>12</sup>A. Pedersen, *IEEE Trans. Power Appar. Syst.* **PAS-94**, 1749 (1975).
- <sup>13</sup>S. Berger, *IEEE Trans. Power Appar. Syst.* **PAS-95**, 1073 (1976).
- <sup>14</sup>W. S. Boyle and P. Kisliuk, *Phys. Rev.* **97**, 255 (1955).
- <sup>15</sup>R. V. Hodges, R. N. Varney, and J. F. Riley (*Phys. Rev. A* in press). [This paper calculates  $P^*$ , the probability of electrical breakdown as a function of the applied voltage  $v$ , as the probability of an infinite avalanche sequence plus the probability of a finite sequence that achieves a critical size. This result can be incorporated into the present paper by letting  $\lambda(v) \rightarrow \lambda(v) = P^*(v)\lambda(v)$  beginning with Eq. (8) below.]
- <sup>16</sup>M. W. Watts, *Proceedings of the 5th International Conference on Gas Discharge*, University of Liverpool, 11–14 Sept. 1978 (IEEE, London, 1978), p. 297.
- <sup>17</sup>R. H. Fowler and L. Nordheim, *Proc. R. Soc. London* **199**, 173 (1928).
- <sup>18</sup>W. B. Davenport, Jr. and W. L. Root, *An Introduction to the Theory of Random Signals and Noise* (McGraw-Hill, New York, 1958), pp. 113–117.
- <sup>19</sup>W. B. Davenport, Jr. and W. L. Root, *An Introduction to the Theory of Random Signals and Noise* (McGraw-Hill, New York, 1958), pp. 32–34.
- <sup>20</sup>M. O. Hagler, A. L. Donaldson, and R. M. Ness, Texas Tech University Pulsed Power Lab Notes, TTU-EEPP-83-1 (1983).
- <sup>21</sup>A. L. Donaldson, M. O. Hagler, M. Kristiansen, G. Jackson, and L. Hatfield, *IEEE Trans. Plasma Sci.* **PS-12**, 28 (1984).
- <sup>22</sup>R. C. Pfaffenberger and J. H. Patterson, *Statistical Methods for Business and Economics* (Irwin, Homewood, IL, 1977), p. 685.
- <sup>23</sup>T. Nitta, N. Yamada, and Y. Fujiwara, *IEEE Trans. Power Appar. Syst.* **PAS-93**, 623 (1974).
- <sup>24</sup>S. Berger, *IEEE Trans. Power Appar. Syst.* **PAS-96**, 1179 (1977).
- <sup>25</sup>C. M. Cooke, *IEEE Trans. Power Appar. Syst.* **PAS-94**, 1518 (1975).
- <sup>26</sup>I. W. McAllister, *Elektrotechn. Z. A* **99**, 283 (1978).
- <sup>27</sup>S. J. Levinson and E. E. Kunhardt, *IEEE Trans. Plasma Sci.* **PS-10**, 266 (1982).
- <sup>28</sup>T. Martin, Sandia National Labs (private communication) (October 1983).
- <sup>29</sup>V. I. Krizhanovskii, A. I. Kuz'michev, G. V. Levchenko, R. B. Luban, and A. I. Shendakov, *Sov. Phys. Tech. Phys.* **26**, 1204 (1981).
- <sup>30</sup>T. J. Lewis, *J. Appl. Phys.* **26**, 1405 (1955).
- <sup>31</sup>J. Jones, *J. Phys. D* **1**, 769 (1968).
- <sup>32</sup>Y. Tzeng and E. E. Kunhardt, 36th Gaseous Electronics Conference (Abstracts), State University of New York, 11–14 Oct. 1983, p. 42.
- <sup>33</sup>J. M. Wozencraft and I. M. Jacobs, *Principles of Communication Engineering* (Wiley, New York, 1965), p. 76.
- <sup>34</sup>J. M. Wozencraft and I. M. Jacobs, *Principles of Communication Engineering* (Wiley, New York, 1965), pp. 129–132.
- <sup>35</sup>J. M. Wozencraft and I. M. Jacobs, *Principles of Communication Engineering* (Wiley, New York, 1965), pp. 135–143.
- <sup>36</sup>L. H. Fisher, *Phys. Rev.* **72**, 423 (1947).
- <sup>37</sup>P. Narbut, E. Berg, C. N. Workes, and T. W. Dakin, *AIEE Trans.* **78**, 545 (1959).
- <sup>38</sup>J. M. Wozencraft and I. M. Jacobs, *Principles of Communication Engineering* (Wiley, New York, 1965), pp. 68–69.
- <sup>39</sup>J. M. Wozencraft and I. M. Jacobs, *Principles of Communication Engineering* (Wiley, New York, 1965), p. 72.
- <sup>40</sup>J. M. Wozencraft and I. M. Jacobs, *Principles of Communication Engineering* (Wiley, New York 1965), p. 77.